ACS OMEGA

http://pubs.acs.org/journal/acsodf

Article

Impact of the *Syn*/*Anti* Relative Configuration of Cryptophane-222 on the Binding Affinity of Cesium and Thallium

Thierry Brotin,* Patrick Berthault, Kévin Chighine, and Erwann Jeanneau

Cite This: *ACS Omega* 2022, 7, 48361−48371

Read Online

ACCESS | Metrics & More | Article Recommendations | Supporting Information

ABSTRACT: We report in this article the synthesis, the X-ray crystal structure of compound *syn*-**2**, and its binding properties with cesium and thallium in aqueous solution under basic conditions. Compound *syn*-**2** is the diastereomeric compound of *anti*-**1** that shows very high affinity for cesium and thallium in aqueous solution under the same conditions. Despite the close structural similarities that exist between the *syn*-**2** and *anti*-**1** compounds, they show large discrepancy in their ability to bind cesium and thallium cations in the same conditions. Indeed, the *syn*-**2** derivative has a lower affinity for these two cationic species and the binding constants are several orders of magnitude lower than those found for its congener. The large differences in affinity observed with these two compounds can be explained by the relative position of the six hydroxyl groups to each other.

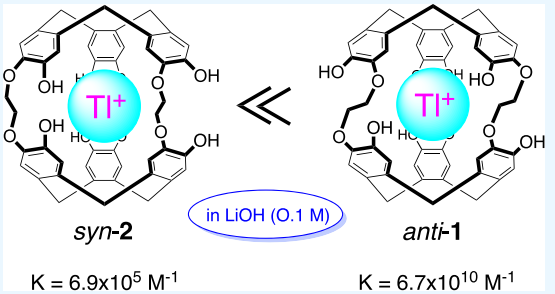

INTRODUCTION

The development of human activities all over the world has strongly modified our planet and the ecosystems in many ways. For instance, it significantly contributed to the pollution of groundwater, soil, and air by toxic substances such as metallic species. Of the various metals involved, thallium has not received as much publicity as mercury and lead, although its toxicity to human health is considered higher.[1] However, nowadays, the danger caused by thallium pollution is well recognized by governmental agencies in different countries and the elimination of this metallic species from groundwater and soil has become a top priority.[2]

Several options have been proposed to recover thallium salts, mainly thallium(I), dispersed in the environment. For instance, mineral matrices seem to be interesting materials to extract thallium from groundwater.[3] These materials are easier to prepare than organic compounds, and they can be produced in larger quantities more easily. On the other hand, non-natural compounds, mainly macrocyclic compounds, with a high affinity for thallium salts have been specifically developed for this purpose.[4] Interestingly, the physical properties of these molecular hosts can be tuned more easily in order to maximize interactions with the cations of interest.

On the other hand, the ^{133}Cs cation is not as toxic as thallium, but the radioactive isotopes of cesium (mainly ^{137}Cs) can represent a significant environmental problem as observed during the Fukushima (2011) and Chernobyl (1986) nuclear accidents. When released in the atmosphere, this species can spread over great distances and contaminate large areas for a long period of time. Many methods to recover ^{137}Cs and decontaminate soils and groundwater have been proposed. For example, different sorbents such as clays, zeolites, and organic compounds including macrocyclic derivatives have been developed for this purpose.[5,6]

Covalently bound molecular capsules, called cryptophanes, decorated with phenol functions exhibit very high affinity for cesium and thallium cations in aqueous solutions under basic conditions.[7] For instance, cryptophane *anti*-**1** bearing six phenol functions shows high binding properties for alkali cations (Rb^+ and Cs^+) and Tl^+ in $LiOH/H_2O$ or $NaOH/H_2O$ (Chart 1). These complexes have been thoroughly studied by different techniques such as ^{133}Cs and ^{205}Tl NMR spectroscopy, electronic and vibrational circular dichroism spectroscopy, or isothermal titration calorimetry (ITC) experiments.

All the cryptophanes studied so far for cesium and thallium complexation possess the relative configuration *anti*. This means that the linkers connecting the two cyclotribenzylene units adopt a helical arrangement. Consequently, the two cyclotribenzylene (CTB) units are tilted from each other and these structures possess an inherent chirality regardless of the nature of the substituents grafted on the six benzene rings. This particular arrangement of the linkers allows the cryptophane to adopt a higher flexibility and to maximize interactions with the encapsulated species.[8] On the other hand, cryptophanes with a small cavity (V_{vdw} < 100 Å^3) and the *syn* configuration have been little described and only a few examples have been

Received: October 12, 2022
Accepted: November 9, 2022
Published: December 15, 2022

https://doi.org/10.1021/acsomega.2c06570
ACS Omega 2022, 7, 48361−48371

Chart 1. Chemical Structures of Compound *Anti*-Cryptophane-A, *Syn*-Cryptophane-B, and Cryptophanes *Anti*-1 and *Syn*-2

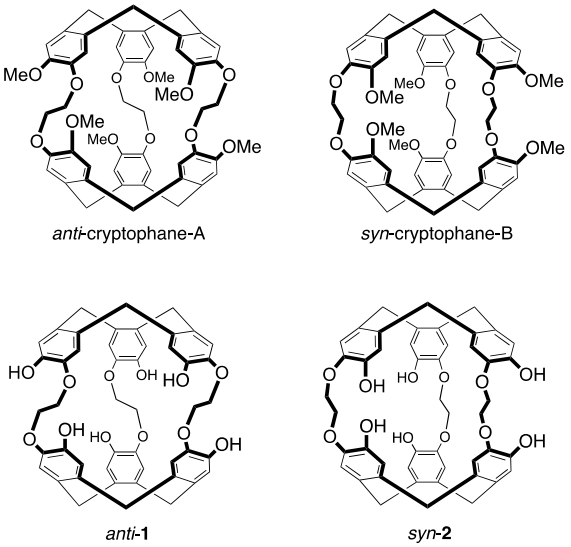

reported in the literature.[9] Recently, a new synthetic approach has allowed us to extend the synthesis to cryptophanes with the *syn* configuration. For example, *syn*-cryptophane-B, the diastereomer of *anti*-cryptophane-A, was prepared in this way (see Chart 1).[10]

Interestingly, the synthetic strategy developed for *syn*-cryptophane-B can also be used to prepare the new *syn*-**2** derivative (Scheme 1), which is nothing but the diastereomer of *anti*-**1** (see Chart 1). At first glance, considering that cesium and thallium cations do not interact with the alkyl chains and that the cavities of *anti*-**1** and *syn*-**2** possess similar volumes, it seems reasonable to assume that compound *syn*-**2** will behave like compound *anti*-**1** in the presence of these two cationic species. Thus, high-binding constants for the Cs^+@*syn*-**2** and Tl^+@*syn*-**2** complexes are also expected with this compound as observed with the *anti*-**1** derivative.

In this work, we report the binding properties of both the Cs^+@*syn*-**2** and Tl^+@*syn*-**2** complexes by means of NMR spectroscopy and ITC. These conditions are identical as those reported in a previous article for the study of the Cs^+@*anti*-**1** and Tl^+@*anti*-**1** complexes. Finally, we compare the results obtained with these two compounds to evaluate the impact of the spatial arrangement of the three $O-CH_2-CH_2-O$ linkers on the molecular recognition properties of this new host.

RESULTS

Synthesis. Hexa-phenol **2** was prepared in a single step from the known derivative *syn*-**3**, the latter being prepared in eight steps from the commercially available 3,4-dihydroxybenzaldehyde.[10]

A hydrogenation step in the presence of a catalytic amount of palladium on charcoal in a CH_2Cl_2/MeOH mixture (50/50: v/v) provided rapidly the desired *syn*-**2** derivative. Extraction with a NaOH (0.5 M)/H_2O solution followed by acidification at 0 °C with few drops of a concentrated HCl solution gave rise to compound *syn*-**2** with 83% yield. This compound can be recrystallized from a hot acetone solution. Compound *syn*-**2** was fully characterized by ^1H and ^{13}C NMR spectroscopy and HRMS. The ^1H NMR spectrum (3.0−9.0 ppm; DMSO-d_6) of **2** is shown Figure 1 and compared to the known hexa-phenol

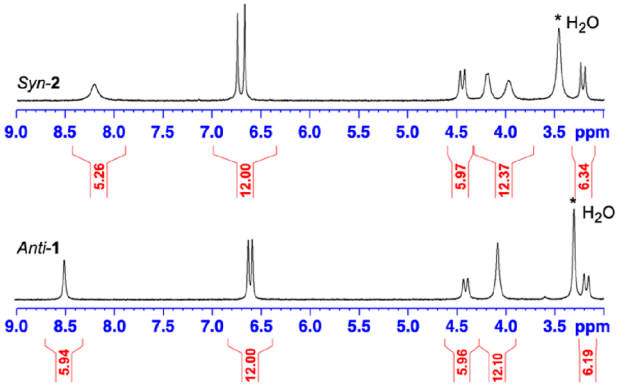

Figure 1. ^1H NMR spectra of compounds *anti*-**1** and *syn*-**2** recorded in DMSO-d_6 at 298 K. The full spectrum of *syn*-**2** (0−10 ppm) is reported in Figure S1.

derivative *anti*-**1**. The two spectra look very similar, with the exception of the diastereotopic protons of compound *syn*-**2**, which appear as two sets of signals instead of one for its congener. ^1H and ^{13}C NMR spectra of compound *syn*-**2** are reported in Figures S1 and S2.

Experimental Procedures. Compound *syn*-**3** (0.38 g, 0.35 mmol) prepared according to a known procedure was introduced in a 50 mL round-bottom flask and dissolved in a mixture of CH_2Cl_2 (12 mL) and MeOH (12 mL) at room temperature.[10] Then, a catalytic amount of Pd/C (10%) was introduced into the flask. The balloon was closed with a septum. Then, hydrogen gas was bubbled into the flask for several minutes and the reaction was kept for 16 h at room temperature under a hydrogen atmosphere. The mixture was filtered over celite, and the solid was washed four times with CH_2Cl_2 and then with a few milliliters of DMSO. The solution was poured into a separating funnel, and the product was

Scheme 1. Synthesis of Compound *syn*-2 from the Tris-phenol Derivative *syn*-3

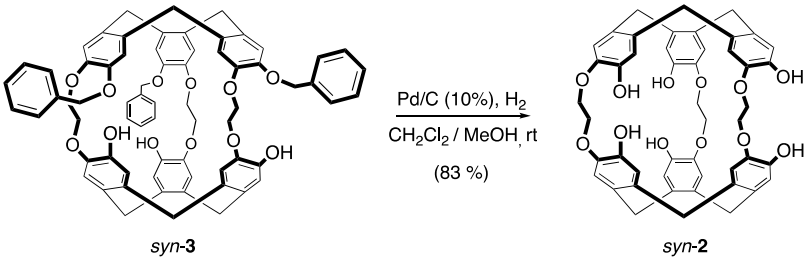

https://doi.org/10.1021/acsomega.2c06570
ACS Omega 2022, 7, 48361−48371

extracted twice with a NaOH (0.5 M)/H_2O solution. The aqueous solution was finally washed four times with CH_2Cl_2 and then cooled down at 0 °C. Acidification with few drops of a concentrated HCl solution gave rise to a white precipitate, which was collected on a frit. The solid was washed with water, dried, and finally washed with diethyl ether to give compound *syn*-**2** as a white powder (0.24 g, 85%). Compound *syn*-**2** crystallized in acetone. Mp: 84 °C. UV−vis (LiOH-0.1 M): λ_{max} (log ε) 340 (4.5 shoulder), 300 (4.27). ^{1}H NMR (300 MHz, DMSO-d_6, 25 °C): δ 8.20 (s, 6H, broad), 6.74 (s, 6H), 6.66 (s, 6H), 4.44 (d, J = 13.2 Hz), 3.35 (m, 12 H, broad), 3.21 (d, J = 13.2 Hz). ^{13}C{^{1}H} NMR (MHz, $CDCl_3$, 25 °C): δ 146.1 (6C), 143.7 (6C), 134.1 (6C), 130.2 (6C), 119.1 (6C), 117.2 (6C), 67.8 (6C), 35.1 (6C). HRMS (ESI) m/z: [M + Na]$^+$ calcd for $C_{48}H_{42}NaO_{12}$: 833,2577; found: 833,2568.

Despite their structural similitude, compounds *anti*-**1** and *syn*-**2** show significant differences in their physical properties. For instance, compared to compound *anti*-**1**, the new derivative *syn*-**2** appears to be only soluble in LiOH/H_2O or NaOH/H_2O solution at a concentration around 0.1 M. At a higher concentration, compound *syn*-**2** precipitates and at a lower LiOH concentration, it gives rise to nano-aggregates as evidenced by diffusion light scattering (DLS). For instance, compound *syn*-**2** dissolved at a concentration of $c = 3 \times 10^{-5}$ M in LiOH/H_2O (10^{-3} M) gives rise to small aggregates whose size is estimated to be 90 nm (Figure S3). This contrasts with compound *anti*-**1** that shows better solubility under these conditions. Thus, all the binding experiments reported with *syn*-**2** in this article will be performed at a LiOH/H_2O and NaOH/H_2O concentration close to 0.1 M.

^{133}Cs NMR Spectroscopy. The ability of compound *syn*-**2** to encapsulate cesium in water under basic conditions was assessed by ^{133}Cs NMR spectroscopy. *Syn*-**2** was dissolved in a 0.1 M NaOD aqueous solution in the presence of an excess of $CsNO_3$ (Figure 2), and ^{133}Cs NMR spectra were recorded as a function of the temperature (275−340 K). At 290 K, the ^{133}Cs NMR spectrum reveals a broad signal at δ = −10 ppm, which has been identified as Cs^+ dissolved in the bulk. We also distinguish another NMR signal located at δ = −130 ppm. Decreasing the temperature up to 275 K allows us to distinguish more easily the second ^{133}Cs NMR signal and to assign this resonance signal to the spectral signature of the Cs^+@*syn*-**2** complex. At 275 K, the Cs^+@*syn*-**2** complex resonates at a higher frequency than the NMR signal observed for the *anti*-**1** congener (δ = −270 ppm). Increasing the temperature decreases the chemical shift splitting between free and bound cesium signals and at 310 K, they coalesce to give a single resonance signal located at δ = −55 ppm. Due to the Eyring relationship (Figure S3), this allows us to calculate an exchange constant $k_{Tc} \approx 1.8 \times 10^4$ s^{-1} and an activation barrier of $\Delta G^{\#}$ = 12.1 kcal.mol^{-1} at this temperature.

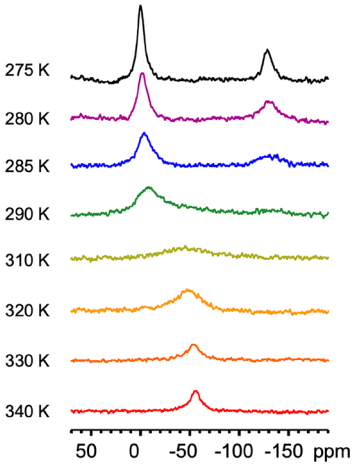

Figure 2. ^{133}Cs NMR spectra of *syn*-**2** dissolved in NaOD (0.1 M)/D_2O in the presence of an excess of $CsNO_3$. Spectra were recorded as a function of temperature (275−340 K).

UV−visible Spectra. Spectroscopic tools such as UV−visible and electronic circular dichroism (ECD) spectroscopy have been very useful to study compound *syn*-**1** and its congeners upon binding with cationic species. However, in contrast to the *anti*-**1** derivative, the achiral structure (C_{3h} symmetry) of this *syn*-**2** prevents us to use ECD spectroscopy to characterize this compound and its complexes. Nevertheless, cryptophanes are made of six benzene chromophores that absorb light below 350 nm, which makes recording their UV−visible spectrum under different conditions possible. Thus, it is possible to detect the symmetry-forbidden ^1L_b transitions of the six benzene rings of cryptophanes that appears near 300 nm. The symmetry-forbidden ^1L_a transition of the benzene chromophore, which is located at lower wavelengths, is also accessible but more difficult to detect because it is buried below the strong symmetry-allowed ^1B_b transition. The UV−visible spectrum of *syn*-**2** in LiOH (0.1 M)/H_2O is reported in Figure S4. This spectrum is very similar to that observed for its congener under the same conditions. For instance, the UV−visible spectrum shows a transition with a maximum at 305 nm that corresponds to the ^1L_b transitions. A shoulder is also observed at lower wavelengths and corresponds to the ^1L_a transitions of the benzene rings. Upon addition of Cs^+ to the solution, the UV−visible spectrum of *syn*-**2** is modified and a slight bathochromic shift of the spectrum is observed. This effect is more pronounced when Cs^+ is replaced by the Tl^+ cation as this was previously observed with its *anti*-**1** congener. Thus, the UV−visible spectra in the presence of these two cations allow us to ascertain that encapsulation of Cs^+ and Tl^+ takes place under these conditions. However, a quantitative description of this phenomenon seems difficult to achieve with this technique and ITC experiments are more appropriate to measure the association constants in this case.

X-ray Structures of Compounds 1−3. X-ray-quality single crystals have been obtained for compounds **1**−**3** in different solvents. Small colorless plate crystals of compound *anti*-**1** suitable for X-ray analysis have been obtained from slow evaporation of a CH_2Cl_2/CH_3CN mixture. Compound *anti*-**1** crystallizes in a monoclinic crystal system and in the $P2_1/c$ space group (Table S1). The unit cell contains four molecules, and each cavity of the host molecules is filled with an acetonitrile molecule. From the ORTEP structure it can be seen that the three O−CH_2−CH_2−O linkers adopt dihedral angles 71.7, −67.8, and 62.2° that are close to those observed for a gauche (g) conformation (Figure 3, Figure S5, and Table S2). This conformation results in a flattened structure of the *anti*-**1** compound where the two CTB caps are staggered with respect to each other. The volume of the internal cavity has been calculated to be 73 Å^3 for this conformation, and the intermolecular cavity has been estimated to be 92 Å^3 (Table S3). It is noteworthy that compound *anti*-**1** also showed residual intermolecular electronic density that could not be modeled by a solvent molecule. The contribution of this

https://doi.org/10.1021/acsomega.2c06570
ACS Omega 2022, 7, 48361−48371

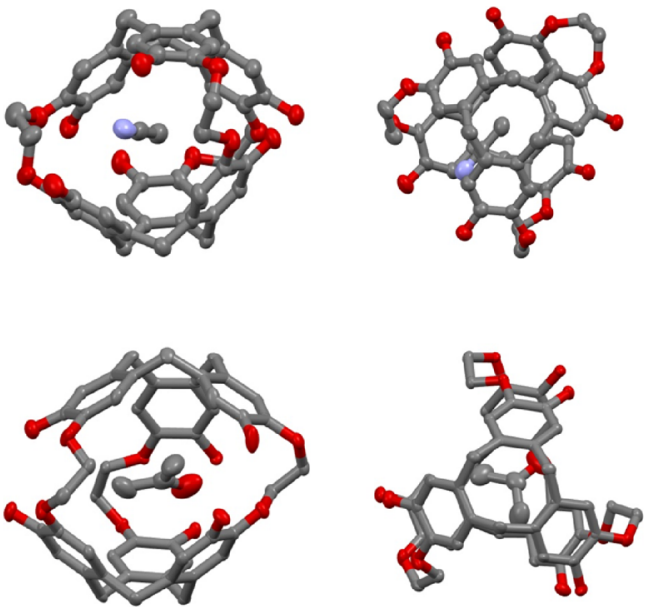

Figure 3. ORTEP representation of compounds CH_3CN@*anti*-**1** (top view) and acetone@*syn*-**2** (bottom view). Two spatial representations are given for each structure. Hydrogen atoms have been removed for clarity. The displacement ellipsoids were plotted at a 30% probability level.

disordered solvent to the structure factors was taken into account with the SQUEEZE algorithm.[11]

We successfully obtained X-ray-quality crystals of compound *syn*-**2** in two different solvents (acetone and acetonitrile). For instance, slow evaporation of an acetone solution provides colorless plate-shaped single crystals of *syn*-**2** suitable for X-ray analysis. In this solvent, compound *syn*-**2** crystallizes in an orthorhombic crystal system and in the *Pbca* space group (Table S1). The unit cell contains eight molecules of *syn*-**2**, and the cavity of the host is filled with an acetone molecule. The interstitial space between molecules has been estimated to be 298 Å^3 and is filled with acetone and water molecules (Table S3). As observed for compound *anti*-**1**, the conformation of the three O−CH_2−CH_2−O linkers is close to that observed for a gauche conformation and dihedral angles of −56.3, 48.3, and 62.6° have been measured from the ORTEP structure (Figure 3, Figure S6, and Table S2). This results in a measured internal cavity V = 93 Å^3 for *syn*-**2**, a value 25% higher than that calculated for the *anti*-**1** compound (Table S3). In pure acetonitrile, compound *syn*-**2** also gives rise to single colorless plate crystals suitable for X-ray analysis. In this solvent, this compound crystallizes in a monoclinic crystal system and in the $P2_1/c$ space group with four molecules per unit cell (Table S1). Both the cavities of the host molecules and the interstitial spaces are filled with acetonitrile molecules. From the ORTEP representation, the internal cavity of the host and the intermolecular voids have been estimated to be V = 91 Å^3 and V = 180 Å^3, respectively (Table S3). This representation (Figure S7) allows us to measure three dihedral angles of 51.9, 62.6, and −54.2° for the three O−CH_2−CH_2−O linkers resulting to angle values very close to those determined previously for the same compound (Table S2). It can be noticed that if we exclude the nature of the guest molecule present in the cavity of *syn*-**2**, the two structures of compound *syn*-**2** in acetone and acetonitrile look very similar.

Finally, single crystals of the intermediate *syn*-**3** suitable for X-ray analysis have been obtained by slow evaporation of a CH_2Cl_2/EtOH solution. Interestingly, in this example, we observed that spontaneous resolution takes place. Compound *syn*-**3** crystallizes in an orthorhombic crystal system and in a $Pca2_1$ space group (Table S1). Near-zero values of the Flack (0.05) and Hooft (0.063) parameters indicate that a single enantiomer is present into the crystal lattice. In our example, the ORTEP representation (Figure 4 and Figure S8)

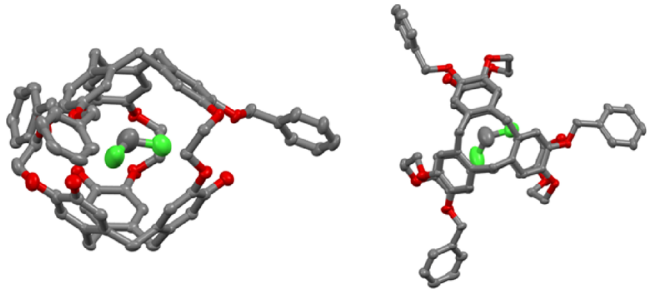

Figure 4. ORTEP representation of compound CH_2Cl_2@*MP-syn*-**3**. The first stereodescriptor refers to CTB decorated with the three phenol groups. The two spatial representations are given for each structure. Hydrogen atoms have been removed for clarity. The displacement ellipsoids were plotted at a 30% probability level. In all these structures, the ORTEP representation reveals the presence of intra- and inter-molecular hydrogen bonding, which have been listed in Tables S4 and S5.

represents the *syn*-**3** derivative with the *MP* absolute configuration, the first letter corresponding to the stereodescriptor of the CTB unit decorated with the OH group. Four molecules are present per unit cell, and the internal cavity of the host molecule (V = 95 Å^3) is filled with a CH_2Cl_2 solvent molecule (Table S3). Large intermolecular voids (V = 305 Å^3) calculated from the ORTEP representation are filled with CH_2Cl_2 molecules. As observed with the previous X-ray structures of compounds *anti*-**1** and *syn*-**2**, the three linkers of *syn*-**3** adopt conformation angles −53.4, 51.0, and 56.8° close to that observed for a gauche (g) conformation (Table S2).

ITC Experiments. ITC is a very efficient method to characterize host−guest interactions under different conditions. This method gives access, in a single experiment, to the stoichiometry of the complex, the binding constant, and the enthalpy of complexation ΔH^0. Thus, the entropy of complexation ΔS^0 and the free energy of complexation ΔG^0 can be easily deduced from these parameters, thereby giving a complete map of the binding process. For instance, titration experiments have been used with success in the case of cryptophane *anti*-**1** and its congeners in the presence of alkali cations and thallium(I) under different conditions.[7b]

In order to compare the binding properties of compound *anti*-**1** with compound *syn*-**2**, a series of ITC experiments were first undertaken with *syn*-**2** in LiOH (0.1 M)/H_2O in the presence of rubidium chloride (RbCl), cesium hydroxide (CsOH), and thallium acetate (TlOAc). The experimental conditions used to study compound *syn*-**2** are similar to those used previously for the *anti*-**1** derivative. Contrary to compound *anti*-**1** that shows good recognition properties for Rb^+, the titration experiments of *syn*-**2** in the presence of Rb^+ in LiOH (0.1 M)/H_2O reveal that this compound does not show any affinity for this cation (Figure S9). In the same solvent, compound *syn*-**2** shows a moderate affinity for the Cs^+

https://doi.org/10.1021/acsomega.2c06570
ACS Omega 2022, 7, 48361−48371

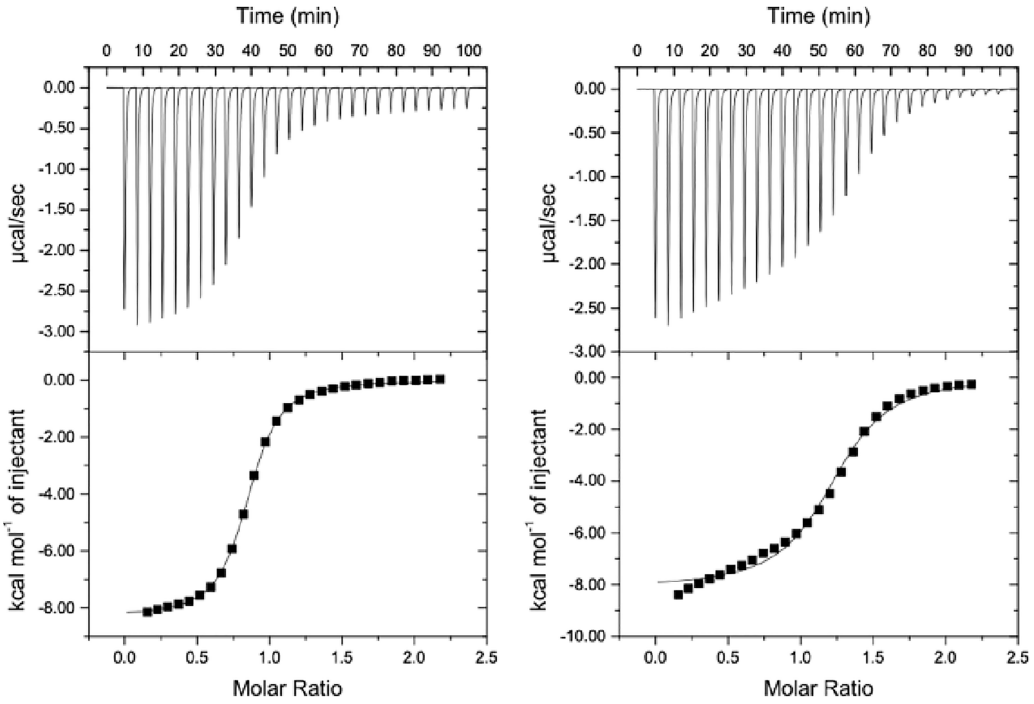

Figure 5. (Left) Isothermal calorimetric titration data (forward titration) of compound *syn*-**2** in LiOH (0.1 M)/H_2O at 298 K. The host solution (c = 0.993 mmol) was placed into the calorimeter cell (1.4 mL), and 28 successive aliquots (10 μL) of TlOAc (c = 0.099 mmol) were added at 3 min intervals (n = 0.8; K = 6.9 × 10^5 M^{-1}; ΔH^0 = −8500 cal·mol^{-1}; ΔS^0 = −1.9 cal·mol^{-1}·K^{-1}; ΔG^0 = −7950 cal·mol^{-1}). (right) Isothermal calorimetric titration data (reverse titration) of compound *syn*-**2** recorded under the same conditions. TlOAc (c = 0.10 mmol) was placed into the calorimeter cell, and 28 successive aliquots (10 μL) of *syn*-**2** (c = 1.02 mmol) were added at 3 min intervals (n = 1.2; K = 3.25 × 10^5 M^{-1}; ΔH^0 = −8100 cal·mol^{-1}; ΔS^0 = −2.0 cal·mol^{-1}·K^{-1}; ΔG^0 = −7500 cal·mol^{-1}).

cation and an association constant K = 1.3 × 10^4 M^{-1} has been measured from the titration experiment (Figure S10). This value appears to be lower by five orders of magnitude than that observed for the Cs^+@*anti*-**1** complex under the same conditions.[7b] In the presence of Tl^+, the situation appears to be different. Indeed, the *syn*-**2** compound shows an enthalpogram that presents the classical S-shape (Figure S11), thus suggesting a strong interaction between *syn*-**2** and this cation. Nevertheless, we failed to fit these experimental points regardless of the fitting model chosen. This difficulty in fitting the experimental data point arises from the fact that the enthalpy of dilution of the Tl^+ cation in LiOH (0.1 M)/H_2O is lower from the enthalpy of dilution of the Tl^+ cation in the presence of *syn*-**2**. Thus, the subtraction of these two enthalpograms results in a small negative enthalpic term that still remains once the cage is fully saturated. Two independent ITC experiments performed under the same conditions give similar results (Figure S11). It is noteworthy that ignoring this small contribution (data points set to zero) leads to a curve that fits perfectly the experimental data to give a binding constant K = 6.9 × 10^5 M^{-1} (ΔG^0 = −8000 cal.mol^{-1}) for the Tl^+@*syn*-**2** (Figure 5). As observed in the case of the Cs^+@*syn*-**2** complex, the binding constant observed in this case is five orders of magnitude lower than the one observed under the same conditions for the Tl^+@*anti*-**1** complex.

Although this procedure has a small impact on the measured binding constant, it remains questionable. Indeed, this small contribution may reflect additional interactions between the Tl^+ cation and *syn*-**2**. In such a case, it is recommended to perform the reverse titration, which requires introduction of the ligand (Tl^+) in the cell and the host molecule (*syn*-**2**) in the syringe.[12] In the case of a classic 1:1 complex such as the one encountered here, we expect the forward and reverse isothermal titrations experiment to be identical. In contrast, a difference between them may reveal a more complex host−guest binding process or additional interactions such as aggregation. It is interesting to note that this procedure was not used with the *anti*-**1** host because in all previously reported examples, the experimental ITC data were fully consistent with a 1:1 complex, regardless of the nature of the cation. However, for comparison, we decided to report in this article the reverse titration of *anti*-**1** with the Rb^+, Cs^+, and Tl^+ performed under the same conditions. A comparison of the reverse titration between these two host molecules seems interesting and can provide additional information about their behavior in the presence of these cationic species.

The reverse titration performed with *syn*-**2** in the presence of Cs^+ shows an experimental ITC curve that fits well with a one-site model. From this experiment, a moderate binding constant K = 7.4 × 10^3 M^{-1} (ΔG^0 = −5300 cal·mol^{-1}) was measured, a value close to that measured for the forward titration (Figure S10). In contrast, replacing Cs^+ with Tl^+ leads to a titration curve more difficult to interpret since the theoretical curve does not fit perfectly well the experimental data (Figure 5). Nevertheless, it should be pointed out that the binding constant K = 3.3 × 10^5 M^{-1} (ΔG^0 = −7500 cal·mol^{-1}) extracted from this experiment is in good agreement with the binding constant measured for the forward titration.

On the other hand, the forward and reverse titrations of compound *anti*-**1** were found identical regardless of the nature of the cation. Thus, the forward and reverse titrations of the Rb^+@*anti*-**1**, the Cs^+@*anti*-**1**, and the Tl^+@*anti*-**1** complexes fit perfectly with a 1:1 complex (Figures S12−S14). For instance, the reverse titration gives a binding constant K = 7.3 × 10^5

https://doi.org/10.1021/acsomega.2c06570
ACS Omega 2022, 7, 48361−48371

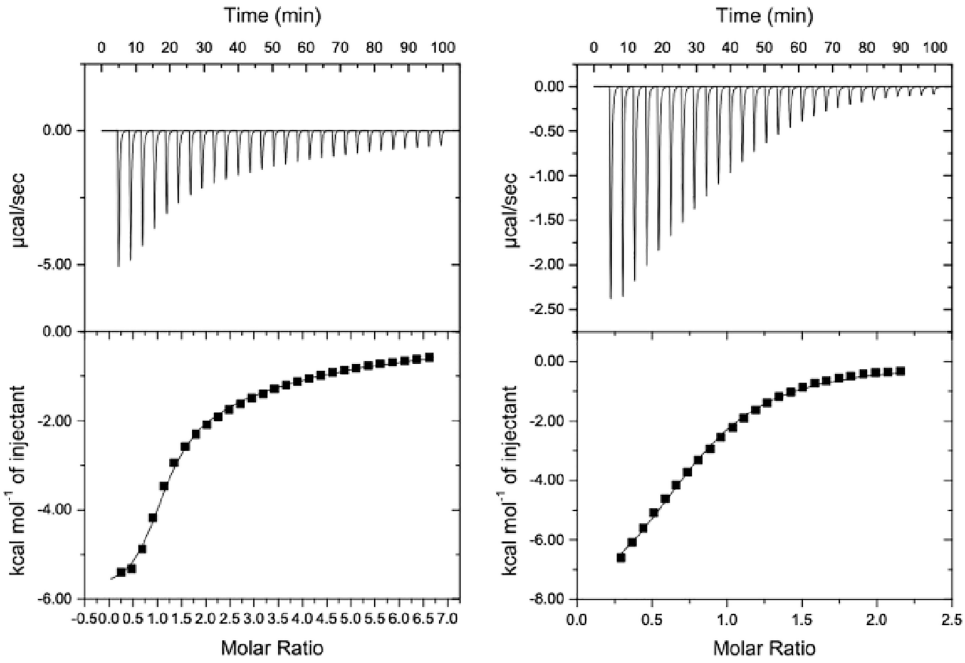

Figure 6. (Left) Isothermal calorimetric titration data (forward titration) of compound *syn*-**2** in NaOH/H_2O-KCl buffer (pH = 12.9) at 298 K. The host solution (c = 0.099 mmol) was placed into the calorimeter cell (1.4 mL), and 28 successive aliquots (10 μL) of TlOAc (c = 3.02 mmol) were added at 3 min intervals (sequential binding site: $K_1 = 1.1 \times 10^5$ M^{-1}; $\Delta H_1^0 = -6100$ cal·mol^{-1}; $\Delta S_1^0 = 2.6$ cal·mol^{-1}·K^{-1}; $\Delta G_1^0 = -6900$ cal·mol^{-1}; $K_2 = 1.8 \times 10^3$ M^{-1}; $\Delta H_2^0 = -15200$ cal·mol^{-1}; $\Delta S_2^0 = -36.1$ cal·mol^{-1}·K^{-1}; $\Delta G_2^0 = -1100$ cal·mol^{-1}). (Right) Isothermal calorimetric titration data (reverse titration) of compound *syn*-**2** recorded under the same conditions. TlOAc (c = 0.1 mmol) was placed into the calorimeter cell, and 28 successive aliquots (10 μL) of *syn*-**2** (c = 0.986 mmol) were added at 3 min intervals (n = 0.8; $K = 6.8 \times 10^4$ M^{-1}; $\Delta H^0 = -8900$ cal·mol^{-1}; $\Delta S^0 = -7.8$ cal·mol^{-1}·K^{-1}; $\Delta G^0 = -6600$ cal·mol^{-1}).

M^{-1} ($\Delta G^0 = -8000$ cal·mol^{-1}) for the Rb^+@*anti*-**1** complex, whereas an association constant $K = 9.2 \times 10^5$ M^{-1} ($\Delta G^0 = -8200$ cal·mol^{-1}) was previously determined for the forward titration.[5b] Similarly, an association constant $K = 8.9 \times 10^8$ M^{-1} ($\Delta G^0 = -12200$ cal·mol^{-1}) was measured for the Cs^+@*anti*-**1** complex instead of $K = 2.7 \times 10^9$ M^{-1} ($\Delta G^0 = -12900$ cal·mol^{-1}) for the reverse reaction. Finally, a binding constant $K = 6.7 \times 10^{10}$ M^{-1} ($\Delta G^0 = -14800$ cal·mol^{-1}) was measured for the reverse titration of the Tl^+@*anti*-**1** complex, a value close to that measured for the forward titration.[7b] Note that in the latter case, the presence of a competitor (Rb^+) was mandatory to accurately measure the association with Tl^+. All together, these results show that compound *syn*-**2** seems to behave differently from compound *anti*-**1** toward cationic species and, upon complexation with thallium, give enthalpograms that are more complex to interpret.

It is important to point out that the titration experiments described above are not performed at constant pH. Indeed, small injection of ligand during the forward and reverse titration experiments slightly modifies the pH of the solution. Thus, a possible change in the pH of the solution may affect the isothermal titration of the *syn*-**2** compound compared to its congener *anti*-**1**. To test this hypothesis, a new series of experiments were performed in a NaOH/KCl buffer to maintain the pH of the solution around pH = 13. For comparison, the titration experiments (forward and reverse) of *anti*-**1** were also performed under the same conditions.

The forward titration of *syn*-**2** shows exothermic heat release upon injection of a small amount of Cs^+ cation in the NaOH/KCl buffer. Using these conditions, a one-site model fits perfectly the data points and allows an estimation of the binding constant $K = 4.1 \times 10^3$ M^{-1} ($\Delta G^0 = -4900$ cal·mol^{-1}) (Figure S15). The reverse titration also results in an enthalpogram that fits well with a one-site model and a binding constant $K = 2.2 \times 10^3$ M^{-1} ($\Delta G^0 = -4600$ cal·mol^{-1}) was extracted from this experiment. A change in the nature of the cation leads to a more complex situation since the addition of Tl^+ to a buffer solution of *syn*-**2** leads to a titration whose data points can only be correctly fitted with two sequential binding sites. Thus, this leads to the determination of two binding constants with different magnitudes $K_1 = 1.1 \times 10^5$ M^{-1} ($\Delta G^0 = -6900$ cal·mol^{-1}) and $K_2 = 1.8 \times 10^3$ M^{-1} ($\Delta G^0 = -4400$ cal·mol^{-1}) (Figure 6). In contrast, the data point fits well with a one-site model for the reverse titration and gives a binding constant of $K = 6.8 \times 10^4$ M^{-1}. We can point out that the first binding constant is consistent with the data measured in LiOH (0.1 M)/H_2O for the forward and reverse experiments.

Under the same conditions, the forward and reverse titrations have been performed with the host *anti*-**1** and the ligands Rb^+, Cs^+, and Tl^+ (Figures S16–S18). In all cases, we noticed that the experimental points fit very well with a 1:1 complex. In addition, both the forward and reverse titrations give similar results. It should be noticed that under these conditions, the binding constants deduced from these experiments are smaller than those previously reported in pure NaOH (0.1 M)/H_2O.[5b] This is because the buffer contains potassium cations present in large excess. Indeed, K^+ shows a moderate affinity (K = 500–1000 M^{-1}) for the host *anti*-**1** and acts as a competitor, thus resulting in lower affinity for the Rb^+@*anti*-**1**, Cs^+@*anti*-**1** and Tl^+@*anti*-**1** complexes (Figure S19) in this solvent.

https://doi.org/10.1021/acsomega.2c06570
ACS Omega 2022, 7, 48361–48371

DISCUSSION

The intermediate *syn*-**3** appears to be a useful derivative to prepare a wide range of C_3-symmetric derivatives with the *syn* configuration due to the presence of three unprotected phenol groups and three other protected phenol functions that allow us to easily modify its structure. For example, recent studies have suggested that cryptophanes with the *syn* configuration possess superior characteristics for the design of ^{129}Xe NMR-based biosensors compared to their *anti*-congeners.[13] Therefore, the interest for the *syn*-compounds should rapidly grow in the future. Interestingly, compound *syn*-**3** allows us to give access to the *syn*-**2** derivative in good yield and in a single step. In our case, this approach was preferred to the demethylation step of *syn*-cryptophane-B with PPh_2Li in THF. Indeed, although this procedure has been successfully used to prepare the *anti*-**1** derivative, the purification step for the *syn*-**2** compound would be more difficult with this approach. For instance, the presence of the large excess of PPh_2Li present in the reaction mixture and the lower solubility of the *syn*-**2** compound would make its purification process more difficult. In addition, *syn*-cryptophane-B also requires the synthesis of the *syn*-**3** derivative to be prepared. Thus, a direct synthesis of *syn*-**2** from compound *syn*-**3** is fully justified in our case. It is worth mentioning that, if necessary, compound *anti*-**1** can also be prepared by this way. Indeed, both *anti*-**3** and *syn*-**3** diastereomers are produced at the same time during the second ring closure reaction and they can be separated from the crude product.[10] However, the synthesis of *anti*-**1** is easier starting from cryptophane-A and larger quantities of this compound can be obtained by this way.

The fact that spontaneous resolution occurs with the *syn*-**3** compound during the crystallization process is also an interesting feature worth discussing. Indeed, the formation of conglomerate has rarely been observed with cryptophanes since most of them crystallize as racemic compounds.[14] Thus, the production of larger quantities of *syn*-**3** would allow us to rapidly isolate the two enantiomers of this cryptophane without the use of costly HPLC methods.[15] It is noteworthy that a large range of new enantiopure derivatives could be obtained by this way.

NMR spectroscopy appeared to be the spectroscopic tool of choice to investigate Cs^+. Due to its large electronic cloud, this heavy atom is known to be very sensitive to a change of their surrounding environment. For instance, in the presence of these two cations, the water-soluble *anti*-cryptophanes show a specific signature, which is usually observable at room temperature. The Cs^+@cryptophane complexes give a specific spectral signature shifted by several hundreds of ppm toward low frequencies on the ^{133}Cs spectrum as a consequence of the strong shielding effect induced by the aromatic ring current. Here, the chemical shift observed for the Cs^+@*syn*-**2** complex is shifted by $\delta = -120$ ppm toward a high frequency, a value significantly lower than the chemical shift observed with the *anti*-**1** congener and other cryptophanes of *anti*-configuration.[7b,c] The higher rigidity of the cryptophane backbone and the larger cavity of the *syn*-**2** allows us to explain this result. Indeed, the *syn*-**2** compound is not able to modify its structure to maximize the interaction with the cesium cation as easily as the *anti*-**1** compound. As a consequence, the shielding effect induced by the aromatic ring current is not as effective as that observed with its congener.

A fast in−out exchange dynamics is also observed with the Cs^+@*syn*-**2** complex above room temperature, leading to a unique ^{133}Cs NMR signal. Decreasing the temperature allows us to slow down the exchange of ^{133}Cs and two distinct NMR signals start to appear at 285 K and below. Thus, in the presence of cesium, compound *syn*-**2** differs significantly from the *anti*-**1** congener. Previously, two distinct behaviors were observed with the water-soluble cryptophanes in the presence of cesium salt.[7c] For cryptophanes showing very high affinity for the Cs^+ cation, a sharpening of the ^{133}Cs NMR signal was observed when increasing the temperature. This is the case of the Cs^+@*anti*-**1** complex that gives rise to a very sharp ^{133}Cs NMR signal at 345 K compared to that observed at room temperature. The sharpening of the ^{133}Cs NMR signal depends on the molecular symmetry of the host. For instance, we have observed that the higher the symmetry of the cryptophane, the sharper the ^{133}Cs NMR signal.[7b,d,16] An opposite effect was observed for cryptophanes showing a moderate or low affinity for the Cs^+ cation, and a sharpening of the ^{133}Cs NMR signal is observed upon decreasing the temperature. For, instance, the Cs^+@cryptophane-233 complex shows this behavior as a function of the temperature.[7b] Our results reveal that the Cs^+@*syn*-**2** complex behaves similarly. Thus, ^{133}Cs NMR spectroscopy allows us to predict whether water-soluble cryptophanes show high or moderate affinity for this cation. Similar experiments were attempted with *syn*-**2** and thallium salts. Unfortunately, in each case, we observed the formation of a precipitate upon addition of a thallium(I) salt, and the liquid-state NMR experiments were impossible.

Despite the structural similarities that exist between the *anti*-**1** and *syn*-**2**, these two compounds differ greatly in their physical properties from a general perspective. Thus, a little change in the arrangement of the $O-CH_2-CH_2-O$ linkers has a strong impact on the overall physical properties of the *syn*-**2** derivative compared to *anti*-**1**. For instance, the solubility properties of *syn*-**2** are significantly modified compared to those of *anti*-**1** under the same conditions and this compound is only soluble in a limited range of pH. On the other hand, the arrangement of the three linkers also modifies significantly the binding properties of compound *syn*-**2** with respect to the *anti*-**1** derivative. Indeed, we observe that the affinity of this host for Cs^+ and Tl^+ cations is decreased by five orders of magnitude with respect to *anti*-**1**. In addition, compound *syn*-**2** does not show any affinity for the Rb^+ cation, whereas a relatively high binding constant $K = 9.2 \times 10^5$ M^{-1} has been measured with the diastereomer *anti*-**1** in LiOH (0.1 M)/H_2O. Thus, despite the presence of six phenol functions grafted on its skeleton, the *syn*-**2** compound behaves like the recently studied C_3-cryptophane derivative whose skeleton is composed only of three phenol functions and three carboxylic acid functions.[7a]

At first sight, a change in the volume of the cavity could be invoked to explain this difference in behavior between these two cryptophanes but we have previously shown that this parameter is not crucial to explain the recognition properties of cationic species by the water-soluble cryptophanes. Indeed, we have shown that *anti*-cryptophanes with cavity volume larger than that of *syn*-**2** show high affinity for the Rb^+, Cs^+, and Tl^+ cations. For instance, a cryptophane-233 derivative possessing one $O-CH_2-CH_2-O$ linker and two $O-CH_2-CH_2-CH_2-O$ linkers still shows good affinity for Rb^+, Cs^+, and Tl^+ with measured binding constants $K = 3.2 \times 10^4$, 4.1×10^7, and 3.7×10^8 M^{-1}, respectively.[7b] Thus, another explanation has to be found to explain this difference of behavior. A previous study

https://doi.org/10.1021/acsomega.2c06570
ACS Omega 2022, 7, 48361−48371

has revealed that the number of phenol groups grafted onto the cryptophane skeleton is pivotal to observe good complexation constants with the Rb^+, Cs^+, and Tl^+ cations.[7c] Thus, a decrease in the number of phenolic functions has a strong impact on the ability of these hosts to bind cationic species. For instance, the water-soluble cryptophane decorated with three phenol groups and three carboxylic acid functions binds moderately the Cs^+ and Tl^+ cations in LiOH (0.1 M)/H_2O.[7a] On the other hand, DFT calculations have suggested that coulombic interactions between the cationic species and the phenolate group play an important role in the stabilization of these complexes.[16] Herein, both *anti*-**1** and *syn*-**2** possess the same number of OH groups and only the spatial arrangement of the phenol functions is modified. Therefore, we must assume that a change in the arrangement of the three O−CH_2−CH_2−O bonds affects the chemical properties of the phenol groups to some extent, making the ionization state of the OH groups more difficult in the case of the *syn*-**2** derivative. The difficulties to deprotonate in part the six OH groups in compound *syn*-**2** could explain both the lower solubility of this derivative compared to the *anti*-**1** derivative and the large difference in the association constants observed between these two derivatives. This assumption seems to be supported by a comparative study of the structure of these two compounds. In the case of *syn*-**2** derivative, it can be observed that the OH groups grafted on its skeleton are facing each other. In contrast, the six phenol functions are eclipsed in the structure of the *anti*-**1** derivative, making them less likely to interact with each other. Consequently, a greater difference in the pK_a of the OH groups should result in the case of the *syn*-**2** derivative compared to the *anti*-**1** derivative. This interpretation seems reasonable and allows us to explain the isothermal titration experiments measured for both compounds *anti*-**1** and *syn*-**2**. Our assumption is also supported by the fact that the forward and reverse titration experiments of compound *syn*-**2** are more sensitive to a small pH change of the solution compared to the *anti*-**1** diastereomer. In addition, different enthalpograms are observed in LiOH (0.1 M)/H_2O and in the NaOH/H_2O-KCl buffer in the case of the thallium complexation for compound *syn*-**2**. In contrast, compound *anti*-**1** does not show such variation and the forward and reverse titration are found to be similar in shape. Unfortunately, this assumption remains difficult to verify experimentally owing to the low solubility of *syn*-**2** in aqueous solutions that prevents an accurate determination of the pK_a of the phenol functions. Furthermore, in the case of *anti*-**1** and *syn*-**2**, the quantum calculations did not allow for accurate determination of the pK_a values of the phenolic functions. The difficulties in fitting the experimental ITC data in the case of the Tl^+@*syn*-**2** complex also raise some questions. Indeed, this problem does not seem to arise for the Cs^+@*syn*-**2** whatever the experimental conditions. It is therefore possible that additional interactions take place with the Tl^+@*syn*-**2** due to its lower solubility, as was the case in the ^{205}Tl NMR studies. Nevertheless, precipitation of this complex does not seem to occur in the cell since the enthalpogram shows a very characteristic pattern in this case.[17] Instead, small aggregates are formed in solution, resulting in additional interactions.

Overall, our results show that a change in the conformation of the O−CH_2−CH_2−O linkers of cryptophanes not only affects the cavity volume and the size of the portals but also modifies the chemical properties of the chemical functions grafted onto the cryptophane skeleton. In the example reported here, a change in the chemical properties of the phenol groups strongly affects the ability of compound *syn*-**2** to accommodate cationic species in basic solutions as easily as its diastereomer *anti*-**1**. Thus, the difficulty for the *syn*-**2** compound to have all six phenol groups fully deprotonated can be suggested to explain the poor binding properties of this compound. As a result, in its ability to bind cationic species, the *syn*-**2** compound has more similarities with a previous cryptophane decorated with only three phenolic functions that moderately binds Cs^+ and Tl^+ than with its *anti*-**1** diastereomer that shows a very high affinity for these two species.

CONCLUSIONS

We report the synthesis and the characterization of cryptophane *syn*-**2** as well as its crystal structure. This compound is the diastereomer molecule of cryptophane *anti*-**1**, which is known to bind very well the cesium and thallium(I) cations in an aqueous solvent. However, despite the structural similarities that exist between these two compounds, our study reveals that from a general point of view, the physical properties of these two derivatives are significantly different. We noticed, for instance, that these two hosts show large differences in their binding properties toward the Cs^+ and the Tl^+ cations. Indeed, isothermal calorimetric titration experiments performed in LiOH (0.1 M)/H_2O or in NaOH/H_2O-KCl buffer reveal that the *syn*-**2** compound has a decreased affinity of several orders of magnitude for these two cations compared to the *anti*-**1** diastereomer studied under the same conditions. In addition, forward and reverse titration experiments of new derivative *syn*-**2** were found more sensitive to small pH variations compared to the *anti*-**1** derivative. To explain this behavior, a larger difference in the pK_a of the phenol functions grafted onto the *syn*-**2** derivative is assumed compared to the *anti*-**1** derivative in which the phenol functions can be more easily ionized at the same pH. This result shows that a change in the linker arrangement not only alters the cavity size and flexibility of the host but also changes the chemical properties of the substituents grafted onto the cryptophane backbone. In turn, this leads to a significant change in the molecular recognition properties of the host.

Overall, the results presented in this paper, in combination with previous studies, show that cryptophanes with an *anti*-configuration exhibit binding of Cs^+ and Tl^+ cations stronger than that of *syn*-congeners. Indeed, while the greater rigidity of *syn*-congeners has most often been cited to explain the weaker binding properties of *syn*-cryptophanes, a change in the physical properties of the substituents grafted onto the benzene rings may also have a strong impact on the binding properties of these derivatives.

EXPERIMENTAL DETAILS

Mass Spectroscopy. Mass spectra (HRMS) were obtained by the Centre de Spectrométrie de Masse, University of Lyon. Analyses were performed with a hybrid quadrupole-time-of-flight mass spectrometer, microToF QII equipped with an electrospray ion source. Data Analysis 4.0 was used for instrument control, data collection, and data treatment. HRMS analyses were performed in full-scan MS with a mass range from 50 to 2000 Da at an acquisition rate of 1 Hz. Transfer parameters were as follows: RF Funnel 1, 200 V; RF Funnel 2, 200 V; hexapole, 50 V; transfer time, 70 μs; and PrePulse storage time, 1 μs. Before each acquisition batch, external

https://doi.org/10.1021/acsomega.2c06570
ACS Omega 2022, 7, 48361−48371

calibration of the instrument was performed with a sodium formate clusters solution. ^{1}H and ^{13}C NMR spectra were recorded at 300 and 75.5 MHz, respectively. Chemical shifts were referenced to Me_4Si (^{1}H and ^{13}C). Column chromatographic separations were carried out over Merck silica gel 60 (0.040−0.063 mm). Analytical thin-layer chromatography (TLC) was performed on Merck silica gel TLC plates, F-254. The solvents were distilled prior to use: DMF and CH_2Cl_2 from CaH_2, THF from Na/benzophenone, and pyridine from KOH.

Single-Crystal X-ray Diffraction. Single-crystals were selected and mounted on an Xcalibur Gemini kappa-geometry diffractometer equipped with an Atlas CCD. Data collections were achieved at 150 K using copper X-ray radiation (l = 1.54184 Å) for *anti*-**1**, *syn*-**2**, and *syn*-**3** and molybdenum radiation (l = 0.71073 Å) for the second X-ray structure of *syn*-**2**. Intensities were collected by means of the CrysalisPro software.[18] Reflection indexing, unit-cell parameter refinement, Lorentz-polarization correction, peak integration, and background determination were carried out with the CrysalisPro software.[18] An analytical absorption correction was applied using the modeled faces of the crystal.[19] The resulting set of *hkl* was used for structure solution and refinement. The structures were solved with the ShelXT structure solution program using the intrinsic phasing solution method and by using Olex2 as the graphical interface.[20,21] The model was refined with version 2018/3 of ShelXL using least-squares minimization.[22]

CCDC 2152416-2152417-2152418-2152419 contains the supplementary crystallographic data for this paper. These data can be obtained free of charge from The Cambridge Crystallographic Date Centre via www.ccdc.cam.ac.uk/data_request/cif.

^{133}Cs NMR Spectroscopy. These experiments were performed on a 11.7 T narrow-bore Bruker spectrometer equipped with a 5 mm BBI probehead and *z*-axis gradient.

■ ASSOCIATED CONTENT

Supporting Information

The Supporting Information is available free of charge at https://pubs.acs.org/doi/10.1021/acsomega.2c06570.

^{1}H and ^{13}C NMR spectra of compound *syn*-**2**, DLS of *syn*-**2** in basic solution, and ITC experiments of *anti*-**1** and *syn*-**2** in LiOH (0.1 M)/H_2O and NaOH/H_2O-KCl (buffer) (forward and reverse experiments) (PDF)

■ AUTHOR INFORMATION

Corresponding Author

Thierry Brotin − *ENSL, CNRS, Laboratoire de Chimie UMR 5182, 69364 Lyon, France;* orcid.org/0000-0001-9746-4706; Email: thierry.brotin@ens-lyon.fr

Authors

Patrick Berthault − *CNRS, CEA, Nanosciences et Innovation pour les Matériaux, la Biomédecine et l'Energie, Université Paris-Saclay, 91191 Gif-sur-Yvette, France;* orcid.org/0000-0003-4008-2912

Kévin Chighine − *CNRS, CEA, Nanosciences et Innovation pour les Matériaux, la Biomédecine et l'Energie, Université Paris-Saclay, 91191 Gif-sur-Yvette, France*

Erwann Jeanneau − *Centre de Diffractométrie Henri Longchambon Université de Lyon 1, 69100 Villeurbanne, France*

Complete contact information is available at: https://pubs.acs.org/10.1021/acsomega.2c06570

Notes

The authors declare no competing financial interest.

■ ACKNOWLEDGMENTS

The French National Research Agency (ANR) is acknowledged for financial support (project ANR19-CE19-0024 PHOENIX).

■ REFERENCES

(1) (a) Campanella, B.; Colombaioni, L.; Benedetti, E.; Di Ciaula, A.; Ghezzi, L.; Onor, M.; D'Orazio, M.; Giannecchini, R.; Petrini, R.; Bramanti, E. Toxicity of Thallium at Low Doses: A Review. *Int. J. Environ. Res. Public Health* **2019**, *16*, 4732−4737. (b) Xiao, T.; Yang, F.; Li, S.; Zheng, B.; Ning, Z. Thallium Pollution in China: A Geo-Environmental Perspective. *Sci. Total Environ.* **2012**, *421*−*422*, 51−58. (c) Peter, A. L. J.; Viraraghavan, T. Thallium: A Review of Public Health and Environmental Concerns. *Environ. Int.* **2005**, *31*, 493−501.

(2) (a) Cvjetko, P.; Cvjetko, I.; Pavlica, M. Thallium Toxicity in Humans. *Arch. Environ. Con. Toxicol.* **2010**, *61*, 111−118. (b) Saha, A. Thallium Toxicity: A Growing Concern. *Indian J. Occup. Health* **2005**, *9*, 53−56. (c) Kazantzis, G. Thallium in the Environment and Health Effects. *Environ. Geochem. Health* **2000**, *22*, 275−280.

(3) (a) López-García, I.; Muñoz-Sandoval, M. J.; Hernández-Córdoba, M. Dispersive Micro-Solid Phase Extraction with a Magnetic Nanocomposite Followed by Electrothermal Atomic Absorption Measurement for the Speciation of Thallium. *Talanta* **2021**, *228*, No. 122206. (b) Liu, J.; Luo, X.; Sun, Y.; Tsang, D. C. W.; Qi, J.; Zhang, W.; Li, N.; Yin, M.; Wang, J.; Lippold, H.; Chen, Y.; Sheng, G. Thallium Pollution in China and Removal Technologies for Waters: A Review. *Environ. Int.* **2019**, *126*, 771−790. (c) Li, H.; Li, X.; Chen, Y.; Long, J.; Zhang, G.; Xiao, T.; Zhang, P.; Li, C.; Zhuang, L.; Huang, W. Removal and Recovery of Thallium from Aqueous Solutions via a Magnetite-Mediated Reversible Adsorption-Desorption Process. *J. Cleaner Prod.* **2018**, *199*, 705−715. (d) Li, H.; Li, X.; Xiao, T.; Chen, Y.; Long, J.; Zhang, G.; Zhang, P.; Li, C.; Zhuang, L.; Li, K. Efficient Removal of Thallium(I) from Wastewater Using Flower-Like Manganese Dioxide Coated Magnetic Pyrite Cinder. *Chem. Eng. J.* **2018**, *353*, 867−877. (e) Huangfu, X.; Jiang, J.; Lu, X.; Wang, Y.; Liu, Y.; Pang, S.-Y.; Cheng, H.; Zhang, X.; Ma, J. Adsorption and Oxidation of Thallium(I) by a Nanosized Manganese Dioxide. *Water, Air, Soil Pollut.* **2014**, *226*, 2272.

(4) (a) Frei, A.; Rigby, A.; Yue, T. T.; Firth, G.; Ma, M. T.; Long, N. J. To Chelate Thallium(I) - Synthesis and Evaluation of Kryptofix-Based Chelators for 201Tl. *Dalton Trans.* **2022**, *51*, 9039−9048. (b) Zhai, H.; Xiong, S.; Peng, S.; Sheng, W.; Xu, G.; Sessler, J. L.; He, Q. Thallium(I) Salts: New Partners for Calix[4]Pyrroles. *Org. Lett.* **2021**, *23*, 2638−2642. (c) Zhao, Z.; Xiong, Y.; Cheng, X.; Hou, X.; Yang, Y.; Tian, Y.; You, J.; Xu, L. Adsorptive Removal of Trace Thallium(I) from Wastewater: A Review and New Perspectives. *J. Hazard. Mater.* **2020**, *393*, No. 122378. (d) Zhao, Z.; Tian, H.; Zhang, M.; Yang, Y.; Zhang, H. Molecular Design of Macrocyclic Compounds for Complete Removal of Thallium(I) from Wastewater. *Environ. Sci. Pollut. Res.* **2018**, *25*, 34550−34558. (e) Makrlík, E.; Dybal, J.; Vaňura, P. Interaction of the Thallium Cation with 1,3-Alternate-25,27-Bis(1-Octyloxy)Calix[4]Arene-Crown-6: Experimental and Theoretical Study. *J. Mol. Struct.* **2013**, *1042*, 73−77. (f) Chester, R. T.; Couton, D.; Lobler, R.; Mocerino, M.; Ogden, M. I.; Pettersen, J. K.; Skelton, B. W.; White, A. H. The extraction of thallium(I) and silver(I) ions with 1,3-alternate calix[4]arene derivatives. *J. Inclusion Phenom. Macrocyclic Chem.* **2011**, *71*, 471−

477. (g) Haddadi, H.; Alizadeh, N.; Shamsipur, M.; Asfari, Z.; Lippolis, V.; Bazzicalupi, C. Cation-π interaction in Complex Formation Between Tl^+ Ion and calix[4]crown-6 and Some calix[4]biscrown-6 Derivatives: Thallium-203 NMR, Proton NMR, and X-ray Evidence. *Inorg. Chem.* **2010**, *49*, 6874−6882. (h) Cuc, D.; Bouguet-Bonnet, S.; Morel-Desrosiers, N.; Morel, J.-P.; Mutzenhardt, P.; Canet, D. Behavior of Cesium and Thallium Cations inside a Calixarene Cavity as Probed by Nuclear Spin Relaxation. Evidence of Cation−π Interactions in Water. *J. Phys. Chem. B* **2009**, *113*, 10800−10807. (i) Roper, E. D.; Talanov, V. S.; Butcher, R. J.; Talanova, G. G. Selective Recognition of Thallium(I) by 1,3-Alternate Calix[4]arene-bis(crown-6 Ether) : A New Talent of the Known Ionophore. *Supramol. Chem.* **2008**, *20*, 217−229. (j) Talanova, G. G.; Roper, E. D.; Buie, N. M.; Gorbunova, M. G.; Bartsch, R. A.; Talanov, V. S. Novel Fluorogenic Calix[4]arene-bis(crown-6-Ether) for Selective Recognition of Thallium(I). *Chem. Commun.* **2005**, 5673−5675. (k) Matthews, S. E.; Rees, N. H.; Felix, V.; Drew, M. G. B.; Beer, P. D. Thallium π-Cation Complexation by Calix[4]tubes: ^{205}Tl NMR and X-ray Evidence. *Inorg. Chem.* **2003**, *42*, 729−734. (l) Parham, H.; Shamsipur, M. Spectrofluorometric Study of Thallium (I) Complexes with Several Macrocyclic Ligands in Methanol Solution. *Talanta* **1993**, *40*, 1353−1356. (m) Yang-Chih, L.; Allison, J.; Popov, A. I. Thallium-205 NMR Study of Tl(I) Macrocyclic Complexes in Nonaqueous Solvents. *Polyhedron* **1985**, *4*, 441−445. (n) Shamsipur, M.; Popov, A. I. Multinuclear Nmr Study of Some Alkali and Thallium Complexes with 1,10-Diaza-18-Crown-6 in Nonaqueous Solutions. *Inorg. Chim. Acta* **1980**, *43*, 243−247. (o) Shamsipur, M.; Rounaghi, G.; Popov, A. I. Sodium-23, Cesium-133 and Thallium-205 NMR Study of Sodium, Cesium and Thallium Complexes with Large Crown Ethers in Nonaqueous Solutions. *J. Solution Chem.* **1980**, *9*, 701−714.

(5) (a) Izosimova, Y.; Gurova, I.; Tolpeshta, I.; Karpukhin, M.; Zakusin, S.; Zakusina, O.; Samburskiy, A.; Krupskaya, V. Adsorption of Cs(I) and Sr(II) on Bentonites with Different Compositions at Different PH. *Minerals* **2022**, *12*, 862. (b) Jiménez-Reyes, M.; Almazán-Sánchez, P. T.; Solache-Ríos, M. Radioactive Waste Treatments by Using Zeolites. A Short Review. *J. Environ. Radioact.* **2021**, *233*, No. 106610. (c) Estelrich, J.; Busquets, M. A. Prussian Blue: A Safe Pigment with Zeolitic-Like Activity. *Int. J. Mol. Sci.* **2021**, *22*, 780. (d) Wang, J.; Zhuang, S. Removal of Cesium Ions from Aqueous Solutions Using Various Separation Technologies. *Rev Environ Sci Biotechnol* **2019**, *18*, 231−269. (e) Figueiredo, B. R.; Cardoso, S. P.; Portugal, I.; Rocha, J.; Silva, C. M. Inorganic Ion Exchangers for Cesium Removal from Radioactive Wastewater. *Sep. Purif. Rev.* **2018**, *47*, 306−336. (f) Johan, E.; Yamada, T.; Munthali, M. W.; Kabwadza-Corner, P.; Aono, H.; Matsue, N. Natural Zeolites as Potential Materials for Decontamination of Radioactive Cesium. *Procedia Environ. Sci.* **2015**, *28*, 52−56. (g) Zhaoyi, T.; Zhaoya, H.; Dong, Z.; Xiaolin, W. Structural Characterization of Ammonium Molybdophosphate with Different Amount of Cesium Adsorption. *J. Radioanal. Nucl. Chem.* **2014**, *299*, 1165−1169.

(6) see for instance: (a) Wang, J.; Zhuang, S. Cesium Separation from Radioactive Waste by Extraction and Adsorption Based on Crown Ethers and Calixarenes. *Nucl. Eng. Technol.* **2020**, *52*, 328−336. (b) Pichierri, F. Macrocycles for the Complexation of Radiocesium: A Concise Review of Crystallographic and Computational Studies. *J. Radioanal. Nucl. Chem.* **2017**, *311*, 1251−1263. (c) Albelda, M. T.; Frías, J. C.; García-España, E.; Schneider, H.-J. Supramolecular Complexation for Environmental Control. *Chem. Soc. Rev.* **2012**, *41*, 3859−3877. (d) Mokhtari, B.; Pourabdollah, K.; Dallali, N. A Review of Calixarene Applications in Nuclear Industries. *J. Radioanal. Nucl. Chem.* **2010**, *287*, 921−934. (e) Wintergerst, M. P.; Levitskaia, T. G.; Moyer, B. A.; Sessler, J. L.; Delmau, L. H. Calix[4]Pyrrole: A New Ion-Pair Receptor As Demonstrated by Liquid−Liquid Extraction. *J. Am. Chem. Soc.* **2008**, *130*, 4129−4139. (f) Casnati, A.; Pochini, A.; Ungaro, R.; Ugozzoli, F.; Arnaud, F.; Fanni, S.; Schwing, M.-J.; Egberink, R. J. M.; de Jong, F.; Reinhoudt, D. N. Synthesis, Complexation, and Membrane Transport Studies of 1,3-Alternate Calix[4]Arene-Crown-6 Conformers: A New Class of Cesium Selective Ionophores. *J. Am. Chem. Soc.* **1995**, *117*, 2767−2777. (g) Mei, E.; Popov, A. I.; Dye, J. L. Complexation of the Cesium Cation by Macrocyclic Polyethers in Various Solvents. A Cesium-133 Nuclear Magnetic Resonance Study of the Thermodynamics and Kinetics of Exchange. *J. Phys. Chem.* **1977**, *81*, 1677−1681.

(7) (a) Brotin, T.; Berthault, P.; Pitrat, D.; Mulatier, J.-C. Selective capture of Thallium and Cesium by a Cryptophane Soluble at neutral pH. *J. Org. Chem.* **2020**, *85*, 9622−9630. (b) Brotin, T.; Goncalves, S.; Berthault, P.; Cavagnat, D.; Buffeteau, T. Influence of the Cavity Size of Water-Soluble Cryptophanes on Their Binding Properties for Cesium and Thallium Cations. *J. Phys. Chem B* **2013**, *117*, 12593−12601. (c) Brotin, T.; Cavagnat, D.; Berthault, P.; Montserret, R.; Buffeteau, T. Water-Soluble Molecular Capsule for the Complexation of Cesium and Thallium Cations. *J. Phys. Chem. B* **2012**, *116*, 10905−10914. (d) Brotin, T.; Montserret, R.; Bouchet, A.; Cavagnat, D.; Linares, M.; Buffeteau, T. High Affinity of Water-Soluble Cryptophanes for Cesium Cations. *J. Org. Chem.* **2012**, *77*, 1198−1201.

(8) Brotin, T.; Dutasta, J.-P. Cryptophanes and Their Complexes—Present and Future. *Chem. Rev.* **2009**, *109*, 88−130.

(9) (a) Doll, M.; Berthault, P.; Léonce, E.; Boutin, C.; Jeanneau, E.; Brotin, T.; De Rycke, N. Study of *syn* and *anti* Xenon-Cryptophanes Complexes Decorated with Aromatic Amine Groups: Chemical Platforms for Accessing New Cryptophanes. *J. Org. Chem.* **2022**, *87*, 2912−2920. (b) Doll, M.; Berthault, P.; Léonce, E.; Boutin, C.; Buffeteau, T.; Daugey, N.; Vanthuyne, N.; Jean, M.; Brotin, T.; De Rycke, N. Are the Physical Properties of Xe@Cryptophane Complexes Easily Predictable? The Case of *syn*- and *anti*-Tris-aza-Cryptophanes. *J. Org. Chem.* **2021**, *86*, 7648−7658. (c) Canceill, J.; Césario, M.; Collet, A.; Guilhem, J.; Riche, C.; Pascard, C. Selective recognition of neutral molecules: ^{1}H n.m.r. Study of the complexation of CH_2Cl_2 and CH_2Br_2 by cryptophane-D in solution and crystal structure of its CH_2Cl_2 cavitate. *J. Chem. Soc., Chem. Commun.* **1986**, 339−341.

(10) Brotin, T.; Jeanneau, E.; Berthault, P.; Léonce, E.; Pitrat, D.; Mulatier, J.-C. Synthesis of Cryptophane-B: Crystal Structure and Study of Its Complex with Xenon. *J. Org. Chem.* **2018**, *83*, 14465−14471.

(11) Spek, L. A. PLATON SQUEEZE: a tool for the calculation of the disordered solvent contribution to the calculated structure factors. *Acta Crystallogr., Sect. A: Found. Crystallogr.allogr., Sect. C: Struct. Chem.* **2015**, *C71*, 9−18.

(12) (a) Herrera, I.; Winnik, M. A. Differential Binding Models for Direct and Reverse Isothermal Titration Calorimetry. *J. Phys. Chem. B* **2016**, *120*, 2077−2086. (b) Grolier, J.-P. E.; Del Rio, J. M. Isothermal Titration Calorimetry: Application of the Gibbs−Duhem Equation to the Study of the Relationship Between Forward and Reverse Titrations. *J. Solution Chem.* **2015**, *44*, 987−1003.

(13) Léonce, E.; Brotin, T.; Berthault, P. *syn*-Cryptophanes: macrocyclic compounds with optimized characteristics for the design of ^{129}Xe NMR-based biosensors. *Phys.Chem.Chem.Phys.* **2022**, *24*, 24793−24799.

(14) Canceill, J.; Cesario, M.; Collet, A.; Guilhem, J.; Riche, C.; Pascard, C. Selective Recognition of Neutral Molecules: ^{1}H NMR Study of the Complexation of CH_2Cl_2 and CH_2Br_2 by Cryptophane-D in Solution and Crystal Structure of Its CH_2Cl_2 Cavitate. *J. Chem. Soc., Chem. Commun.* **1986**, 339−341.

(15) Jacques, J.; Collet, A.; Wilen, S. H. *Enantiomers, Racemates, and Resolutions*; Wiley: New York, 1981.

(16) Chapellet, L. L.; Dognon, J.-P.; Jean, M.; Vanthuyne, N.; Berthault, P.; Buffeteau, T.; Brotin, T. Experimental and Theoretical Study of the Complexation of Cesium and Thallium Cations by a Water-Soluble Cryptophane. *ChemistrySelect* **2017**, *2*, 5292−5300.

(17) Eggers, D. K.; Fu, S.; Ngo, D. V.; Vuong, E. H.; Brotin, T. Thermodynamic Contribution of Water in Cryptophane Host−Guest Binding Reaction. *J. Phys. Chem. B* **2020**, *124*, 6585−6591.

(18) *Rigaku Oxford Diffraction, CrysAlis(Pro) Software system, version 1.171.40.67a*, Rigaku Corporation: Oxford, UK. 2019

https://doi.org/10.1021/acsomega.2c06570
ACS Omega 2022, 7, 48361−48371

(19) Clark, R. C.; Reid, J. S. The analytical calculation of absorption in multifaceted crystals. *Acta Crystallogr., Sect. A: Found. Crystallogr.* **1995**, *A51*, 887−897.
(20) Sheldrick, G. M. SHELXT − Integrated space-group and crystal-structure determination. *Acta Crystallogr., Sect. A: Found. Crystallogr.* **2015**, *A71*, 3−8.
(21) Dolomanov, O. V.; Bourhis, L. J.; Gildea, R. J.; Howard, J. A. K.; Puschmann, H. OLEX2: a complete structure solution, refinement and analysis program. *J. Appl. Crystallogr.* **2009**, *42*, 339−341.
(22) Sheldrick, G. M. Crystal structure refinement with SHELXL. *Acta Crystallogr., Sect. A: Found. Crystallogr.allogr., Sect. C: Struct. Chem.* **2015**, *C27*, 3−8.

https://doi.org/10.1021/acsomega.2c06570
ACS Omega 2022, 7, 48361−48371